Efficient autocatalytic reactive mixing and solitary chemical waves in laminar flows

Thomas D. Nevins,[1] Daniel E. Troyetsky,[2] and Douglas H. Kelley[2,*]
[1]*Department of Physics & Astronomy, University of Rochester, Rochester, New York 14627, USA*
[2]*Department of Mechanical Engineering, University of Rochester, Rochester, New York 14627, USA*

(Received 7 November 2019; accepted 11 June 2020; published 24 June 2020)

Reactive mixing, in which fluid flow affects the dynamics of a chemical or biological process by continually altering local concentrations, is common in industrial systems. Often a key design goal is to generate reaction products as quickly as possible while expending minimal energy to drive the flow. In systems like microfluidic devices, where turbulence is inaccessible, efficient reactive mixing requires choosing flows carefully. Here we compare product generation rates of an autocatalytic reaction in a collection of steady, laminar shear flows, all with the same kinetic energy, to each other and to the case of reaction without flow. The resulting advection-reaction-diffusion dynamics are estimated by tracking reaction fronts using the computationally inexpensive eikonal approximation, then simulated directly; the two approaches agree closely. Prior studies noted that reaction fronts in Poiseuille flow converged over time to steady shapes that advance at constant speed (solitary chemical waves), and we find the same phenomenon in all the flows considered. Observing that solitary waves advance at speeds dependent on flow velocity extrema, we construct an analytic model that accurately predicts their shape and speed from the flow velocity profile and chemical front speed. The model implies that concentrating kinetic energy in a narrow region maximizes product generation, and we validate that prediction with further simulations. We show that in the case of solitary waves with speed zero, the model reproduces prior theoretical, experimental, and numerical studies of frozen fronts. By simulating full advection-reaction-diffusion dynamics, we find that the eikonal approximation predicts the size of the reacted region within a few percent and predicts the converged product generation rate within a few tenths of a percent.

DOI: 10.1103/PhysRevFluids.5.063201

I. INTRODUCTION

Industrial and biological systems frequently involve reactive mixing, in which chemical reaction and/or biological growth proceeds in the presence of a fluid flow, resulting in some chemical product. Since flow can advect catalysts to unreacted materials, flow can promote reaction to generate greater amounts of chemical products in less time. However, driving flow requires adding kinetic energy to the system, usually at some cost; an optimal flow generates products as quickly as possible while requiring minimal energy. Designing such a flow is not trivial, particularly in cases when system size, material properties, or chemical constraints prevent the imposition of turbulence. Misunderstandings of reactive mixing in the chemical process industry leads to problems in scaleup and in wasted energy [1,2]. Though mixing effectiveness can be quantified by multiple measures [3], research in industrial reactive mixing is often restricted to empirical studies of a given reactor design, either through small-scale tests, full-scale tests, or direct numerical simulation [4,5]. Indeed,

*d.h.kelley@rochester.edu

TABLE I. The first five flows considered, along with stagnant fluid. For each of the five, the total kinetic energy [Eq. (1)] is K.

Description	Flow velocity
Couette flow	$u = \sqrt{\frac{24K}{h}}\left(\frac{y}{h} - \frac{1}{2}\right)$
Poiseuille flow	$u = \sqrt{\frac{1440K}{h}}\left(-\frac{y^2}{2h^2} + \frac{y}{2h} - \frac{1}{12}\right)$
Second-order shear flow	$u = \sqrt{\frac{8064K}{h}}\left(\frac{y^3}{3h^3} - \frac{y^2}{2h^2} + \frac{y}{4h} - \frac{1}{24}\right)$
Sine flow	$u = \sqrt{\frac{4K}{h}}\sin\frac{2\pi y}{h}$
Cosine flow	$u = -\sqrt{\frac{4K}{h}}\cos\frac{2\pi y}{h}$
Stagnant	$u = 0$

general frameworks have been devised for mixing passive scalars [6–9], but for reactive mixing, general results are rare [3,10].

Here, with optimal design of laminar chemical mixers in mind, we consider the reactive mixing caused by a collection of laminar flows. We intentionally consider simple flows where intuition, theoretical analysis, and simulation can all provide insight that might later be applied to more complex and realistic situations. We begin with the five flows listed in Table I, comparing the product generation rate in each to the generation rate in stagnant fluid. Each flow imposes shear in a two-dimensional domain $0 \leqslant y \leqslant h$ in the (x, y) plane. We use Cartesian coordinates throughout, with unit vectors $(\hat{\boldsymbol{x}}, \hat{\boldsymbol{y}})$. Each flow has a velocity profile of the form $\boldsymbol{u} = u(y)\hat{\boldsymbol{x}}$, all of which are shown in Fig. 1. Such flows involve only streamwise flow and specifically lack vortices, which can act as barriers to mixing. Our flows include important cases like Couette and Poiseuille flows, which arise frequently in common geometries. In each case, there is no mean flow: $\int_0^h u\,dy = 0$. Accordingly, the form of Poiseuille flow we consider has nonzero velocity at the boundaries and is related by a change of reference frame to Poiseuille flow with stationary, no-slip boundaries.

The central question of our investigation is straightforward: if the total kinetic energy,

$$K = \frac{1}{2}\int_0^h u^2 dy, \tag{1}$$

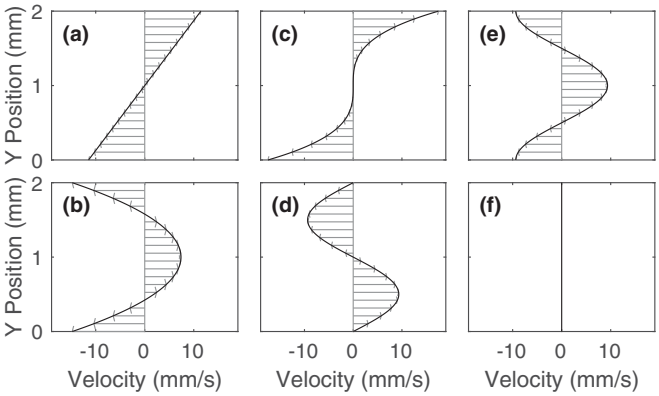

FIG. 1. Velocity profiles of the first five flows considered, all in the frame of reference in which their mean is zero, along with stagnant fluid: (a) Couette flow, (b) Poiseuille flow, (c) second-order shear flow, (d) sine flow, (e) cosine flow, and (f) stagnant fluid.

is held constant, does the functional form of $u(y)$ affect the rate at which reaction products are generated, once transient effects disappear? If so, what form maximizes the product generation rate? More specifically, with intuition that fast flow may promote reaction better than slow flow, are products generated more quickly with a sharper velocity profile that involves higher local speeds or a smoother profile in which the average speed is higher? Answers could give insight into improving reactor design and guide engineers toward flows that use energy most efficiently.

The velocity profiles we consider are realistic in that they satisfy $\boldsymbol{\nabla} \cdot \boldsymbol{u} = 0$; for incompressible fluids, these profiles conserve mass. However, we do not focus on the mechanisms for driving these shear flows, nor do we solve the Navier-Stokes equation that governs their momentum. Rather, we prescribe the velocity profiles and focus on understanding the reactive mixing they cause. Once desirable velocity profiles have been identified, finding mechanisms to produce them, exactly or approximately, can be addressed in detail in future work. Body forces imposed electromagnetically can produce a wide range of potentially useful flows, for example. Crucially, any flow designed for reactive mixing requires kinetic energy that must be supplied by the mixer, so we keep energy in mind throughout this work.

Reactive mixing is governed by the advection-reaction-diffusion equation,

$$\frac{\partial c}{\partial t} + (\boldsymbol{u} \cdot \boldsymbol{\nabla})c = \alpha F(c) + D\nabla^2 c, \tag{2}$$

where $0 \leqslant c \leqslant 1$ is the dimensionless product concentration that varies through space and time, t is time, α is the reaction rate, $F(c)$ specifies the chemical kinetics, and D is the material diffusivity. We consider second-order chemical kinetics $F(c) = c(1-c)$ because it is the simplest form that has equilibria at $c = 0$ and $c = 1$. If the velocity u is specified, then the dynamics are governed by two dimensionless parameters, which can be written as two Damköhler numbers. The first Damköhler number, defined as $\mathrm{Da_I} = \alpha h/U$, where $U = \sqrt{2K/h}$ is the root-mean-square velocity, gives the ratio of the advection timescale to the reaction timescale. The second Damköhler number, defined as $\mathrm{Da_{II}} = \alpha h^2/D$, gives the ratio of the diffusion timescale to the reaction timescale. In the cases considered here, the second Damköhler number $\mathrm{Da_{II}}$ is equivalent to the Thiele number Φ^2. By defining the dimensionless quantities $\tilde{\boldsymbol{u}} = \boldsymbol{u}/U$, $\tilde{\boldsymbol{\nabla}} = h\boldsymbol{\nabla}$, and $\tilde{t} = tU/h$, Eq. (2) can be written in dimensionless form:

$$\frac{\partial c}{\partial \tilde{t}} + (\tilde{\boldsymbol{u}} \cdot \tilde{\boldsymbol{\nabla}})c = \mathrm{Da_I} F + \frac{\mathrm{Da_I}}{\mathrm{Da_{II}}} \tilde{\nabla}^2 c.$$

Equation (2) is a nonlinear partial differential equation for which general analytic solutions are unknown. Moreover, numerical simulations are often computationally expensive, because in realistic problems, the advection, reaction, and diffusion timescales often differ by many orders of magnitude. However, in the limiting case $\mathrm{Da_{II}} \gg 1$, in which the reaction timescale is much shorter than the diffusion timescale, the reaction dynamics are essentially confined to narrow reaction fronts that separate reacted regions from unreacted regions. In that case, the dynamics of the two-dimensional field $c(\boldsymbol{x}, t)$ reduces to the dynamics of the reaction fronts, a discrete set of one-dimensional curves (or two-dimensional surfaces in systems with three spatial dimensions). The eikonal approximation asserts that the reaction fronts advance with velocity $\boldsymbol{w}$ according to a superposition of the underlying flow velocity and an inherent chemical front velocity v_0:

$$\boldsymbol{w} = \boldsymbol{u} + v_0 \hat{\boldsymbol{n}}. \tag{3}$$

Here $\hat{\boldsymbol{n}} = \hat{\boldsymbol{x}} \sin\theta - \hat{\boldsymbol{y}} \cos\theta$ is the unit vector locally normal to the front and pointing in the direction the front would advance in the absence of advection ($\boldsymbol{u} = 0$), that is, in the direction of $-\boldsymbol{\nabla} c$. We label the angle between the front and the x axis as θ. We have neglected the effect of front curvature, which we will discuss below. In the specific case of an advection-reaction-diffusion system with just one spatial dimension, $F(c) = c(1-c)$, and $\boldsymbol{u} = 0$, Eq. (2) has an analytic solution that takes the form of a solitary chemical wave with velocity [11,12]:

$$v_0 = 5(\alpha D/6)^{1/2}. \tag{4}$$

In dimensionless terms, $v_0/U = 5\sqrt{\mathrm{Da}_I}/\sqrt{6\mathrm{Da}_{II}}$. Using this eikonal approximation to design for efficient autocatalytic mixing has been suggested elsewhere [13] but has not been attempted to our knowledge. Asserting a constant chemical velocity v_0 even when $\boldsymbol{u} \neq 0$ is an ansatz that has proved accurate in a wide variety of situations, including those described below.

Flow always displaces fronts, as specified by Eq. (3), and if shear is present, flow also rotates fronts. For flows of the form $\boldsymbol{u} = u\hat{\boldsymbol{x}}$, the displacement and rotation rates of chemical fronts in the eikonal approximation are given by three ordinary differential equations [14]:

$$\begin{aligned} \boldsymbol{w} \cdot \hat{\boldsymbol{x}} &= u + v_0 \sin\theta \\ \boldsymbol{w} \cdot \hat{\boldsymbol{y}} &= -v_0 \cos\theta \\ \frac{\partial\theta}{\partial t} &= -\frac{\partial u}{\partial y} \sin^2\theta. \end{aligned} \tag{5}$$

The first two expressions govern the rate of change of a front element's position; the third, its angle. Equations (5) often allow greater intuition and easier analytic progress than Eq. (2). For example, they make it clear that increasing the local flow speed u increases one component of the front velocity and therefore the product generation rate, as will be considered more carefully below. They can also be solved numerically with far less computational expense. Their solutions reproduce observed phenomena, including frozen fronts [15], pinning to an obstacle [16], and an anomalous apparent front speed in thin-layer experiments [17]. Thus we shall use the eikonal approximation to study the efficiency of reactive mixing in two-dimensional shear flows. We reiterate, however, that Eqs. (5) are valid only in the $\mathrm{Da}_{\mathrm{II}} \gg 1$ case.

The remainder of the paper proceeds as follows: Section II describes our numerical methods for simulating front dynamics using the eikonal approximation and then presents the results of those simulations. Section III points out that leading elements of fronts play an important role, uses that realization to predict the shapes of the solitary chemical waves to which fronts converge, and presents a flow that is nearly optimal for reactive mixing. To further validate the results of our eikonal simulations and our analytic predictions, we simulated the full advection-reaction-diffusion dynamics; our methods and results are described in Sec. IV. Section V summarizes our results, discusses some implications and limitations, and suggests related future work.

II. EIKONAL SIMULATION

We begin our study of efficient autocatalytic mixing by numerically solving Eqs. (5) for each of the flows listed in Table I to explore the dynamics of their reaction fronts and product generation rates using the eikonal approximation. We use fourth-order Runge-Kutta time stepping in a domain that is unbounded in the x direction and spans $0 \leqslant y \leqslant h$. We use a regular, one-dimensional grid with spacing $h/2000$ or smaller. Spatial gradients are calculated using central differences. We initialize fronts as lines at $x = 0$ at time $t = 0$, with $\theta = \pi/2$ (rightward fronts) and $\theta = -\pi/2$ (leftward fronts), then study the growth of the reacted region that forms between them. When front elements leave the domain by moving to locations $y > h$ or $y < 0$, we use a cubic scheme to resample the front elements within the simulation domain, thereby keeping the grid constant. We choose the time step using a Courant-Friedrichs-Lewy number equal to 0.15. We choose $v_0 = 0.072$ mm/s to match the chemical front speed of the Belousov-Zhabotinsky (BZ) reaction, whose chemical kinetics have been carefully measured [18]. Though the BZ reaction is a complicated chemical system whose precise behavior involves multiple species [19,20], fitting to a single-component model gives an effective reaction rate $\alpha = 1.2\ \mathrm{s}^{-1}$ and effective diffusivity $D = 1.0 \times 10^{-3}\ \mathrm{mm}^2/\mathrm{s}$ [21], consistent with $v_0 = 0.072$ mm/s according to Eq. (4). We choose $h = 2$ mm with microfluidic and small-scale industrial mixers in mind, resulting in $\mathrm{Da}_{\mathrm{II}} = 4800$ for all cases considered below. We continue each simulation long enough for the growth rate of the reacted region to converge. The total kinetic energy [Eq. (1)] is $K = 43.7\ \mathrm{mm}^3\,\mathrm{s}^{-2}$ for all flows, a value similar to prior laboratory experiments. Its units reflect that in precise terms, it is the kinetic

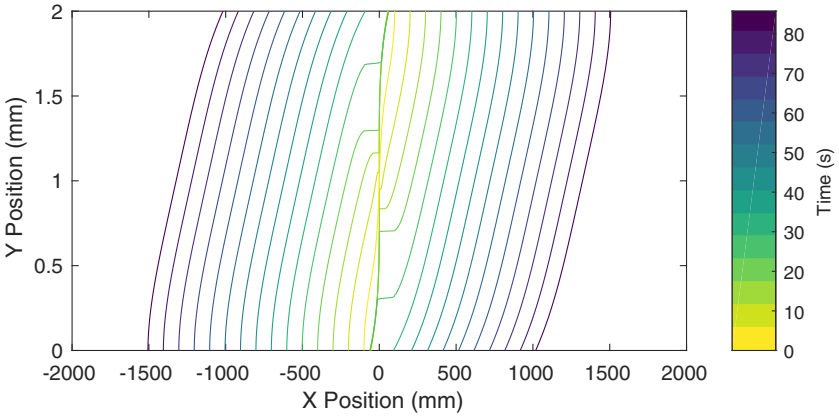

FIG. 2. Reaction fronts advancing over time according to eikonal dynamics in second-order shear flow. As the reacted region grows, the left and right fronts that form its boundaries separate, moving faster where their motion is supported by the flow and slower where opposed. Cusps arise where the fronts are pinned. The same front motion is animated in the Supplemental Material, movie S1 [22].

energy per unit mass, integrated over the spanwise direction. For brevity, we shall refer to it simply as the total kinetic energy. According to Eq. (1), the first Damköhler for each flow is given by

$$\mathrm{Da}_\mathrm{I}^2 = \frac{\alpha^2 h^3}{2K} \int_0^1 \tilde{u}^2 d\tilde{y},$$

where $\tilde{y} = y/h$.

The simulations produce reacted regions that grow over time as rightward and leftward fronts advance. One example is illustrated in Fig. 2, which shows fronts in second-order shear flow at times ranging from $t = 0$ to $t = 85.7$ s ($\tilde{t} = 283$). The same fronts are animated in the Supplemental Material, movie S1 [22]. In regions where $\boldsymbol{u} \cdot \hat{\boldsymbol{n}} > 0$ ("supporting" flow), fronts quickly advance from their initial position at $x = 0$. In regions where $\boldsymbol{u} \cdot \hat{\boldsymbol{n}} < 0$ ("opposing" or "adverse" flow), fronts linger longer and sometimes retreat, as in prior studies that predicted or observed fronts being frozen by headwinds [13,15,23]. Cusps, which are common in front dynamics and have been shown by prior studies to play an important role in the physics [13,24], first develop at the boundaries between regions where these two conditions apply. In this flow, the regions of advancing fronts eventually grow to fill the domain and the cusps disappear. After sufficient time, each front converges on a shape that persists as long as the simulation continues and propagates at constant speed. Those converged fronts are solitary waves (solitons), predicted and observed previously in Poiseuille flow [23,25]. We find that fronts converge to solitary waves, not only in Poiseuille flow but also in all other flows considered, including the second-order shear flow depicted in Fig. 2.

The persistence of solitary waves suggested that they are robust, so we tested their dynamic stability. After simulating for long enough that the front shape had converged, we perturbed the shape by shearing it 30% in the x direction. When we used the perturbed shape as the initial condition in a new simulation, we found that the front returned to the unperturbed converged shape, as shown in Fig. 3. Our observation that these solitary waves are dynamically stable is consistent with prior observations of similar solitary waves in simulations and experiments [17,23,25,26], because if they were unstable, the likelihood of observing them would be negligible. Our observation also generalizes a prior observation that frozen fronts are stable [13], since frozen fronts can be understood as solitary waves of speed zero, or equivalently, solitary waves can be understood as frozen fronts in a different frame of reference.

Solitary wave shapes for all six of the cases listed in Table I are shown in Fig. 4. In Couette flow and sine flow, as in second-order shear flow, corners appear as a transient effect but are eliminated

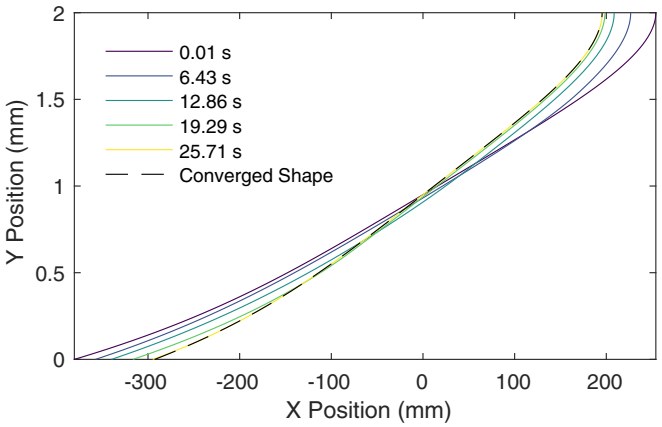

FIG. 3. Front shape stability. If the shape of a converged front is perturbed by shear and then used as the initial condition for a new simulation, the front returns to its converged shape as time goes on, as shown.

from the fronts as they converge, and the solitary waves are smooth. In Poiseuille flow and in cosine flow, however, competing regions are balanced in a way that causes cusps to persist indefinitely; they are visible in the solitary wave shapes. Persistent cusps are consistent with prior predictions [23] and observations [25] for Poiseuille flow. The analysis of [13] uses different terminology but makes the related prediction that frozen fronts (which are solitary waves moving at speed zero, as we will discuss below) can contain corners, showing examples from simulation and experiment. The cusps we observe here are sharp; accounting for the effect of front curvature in Eq. (3) would round their tips but not eliminate them.

Figure 4 also shows that different flows produce reacted regions of different sizes: some flows are more efficient for reactive mixing. The reacted regions formed by all five flows with finite kinetic energy are much larger than the region formed in stagnant fluid ($K = 0$). In that case, the fronts persist as straight lines and the reacted region grows at a rate $2v_0$, so its width at $t = 67.6$ s, the

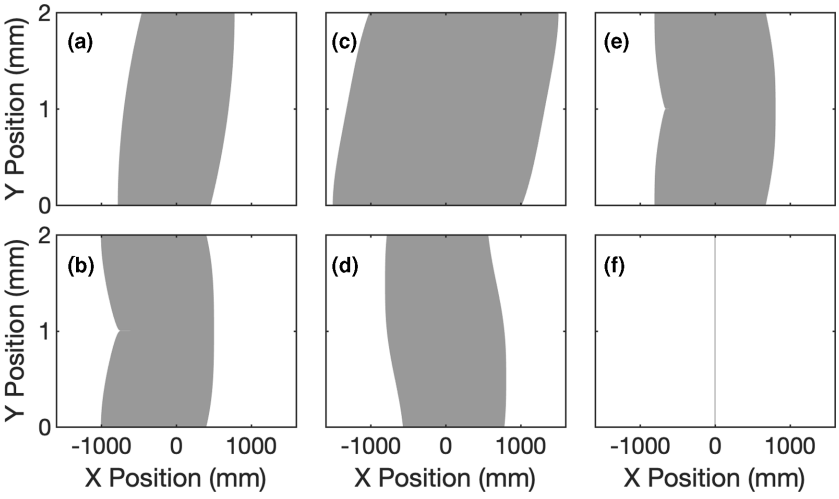

FIG. 4. Solitary wave shapes in the six flows considered, from numerical solutions of Eqs. (5), all at time $t = 67.6$ s ($\tilde{t} = 223$): (a) Couette flow, (b) Poiseuille flow, (c) second-order shear flow, (d) sine flow, (e) cosine flow, and (f) stagnant fluid. Reacted regions are shaded, and the field of view is the same for all six plots.

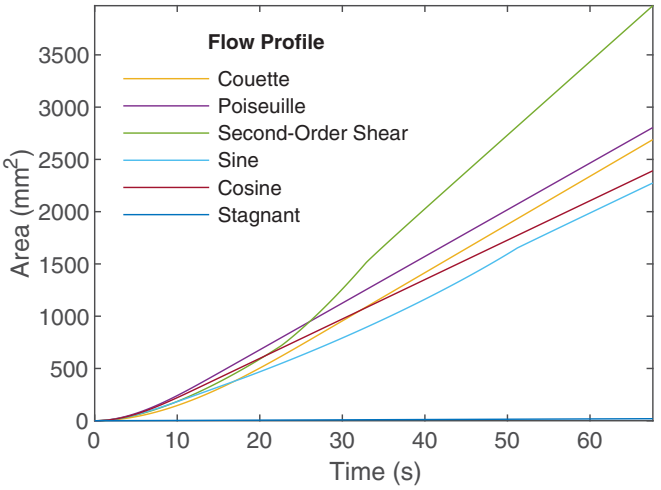

FIG. 5. The reacted regions grow over time in all six flows but at different rates. Without flow, only chemical kinetics drives growth, so it is slow. Sudden changes in growth rate occur when corners leave the domain. In all six cases, after the front shapes have converged the reacted regions grow at a constant rate such that the plots asymptotically approach straight lines. Their slopes determine the reactive mixing efficiency.

moment shown in Fig. 4(a), is 9.73 mm $= 4.87h$, almost vanishingly small compared to the other reacted regions.

Since we are interested in the product generation rate, we investigate the area of the reacted region as it evolves over time, for each of the six cases, as plotted in Fig. 5. The area grows monotonically in all cases, though far slower in the case of stagnant fluid. The rate of change of area approximately equals the product of the total front length and the chemical velocity v_0, though in simulations, measuring area is likely more accurate. When flow is present, the area grows slowly initially before growing more rapidly at later times. In fact, as the front converges to a solitary wave at long times, the rate of change of reacted area $\partial A/\partial t$ converges to a constant growth rate, different in each case. Thus the curves in Fig. 5 asymptotically approach lines of different slopes. Those converged slopes are listed in Table II. Among the six cases, growth is fastest in second-order shear flow. Poiseuille flow and Couette flow have smaller converged growth rates. The growth rate caused by Poiseuille flow is consistent with the effective reaction front speed observed in Poiseuille flow in prior work [23,25]. The smallest is the growth rate caused by sine and cosine flow, which cause growth at the

TABLE II. Converged growth rates of reacted regions, along with efficiency, maxima, and minima of velocity profiles, and the converged growth rate predicted by pinning to leading elements as described in Sec. III. The efficiency of growth in stagnant fluid is undefined. In all cases, the measured converged growth rate matches the prediction.

Description	$\partial A/\partial t$ (mm^2/s)	η	$u_{\max}$ (mm/s)	$u_{\min}$ (mm/s)	$h(u_{\max} - u_{\min} + 2v_0)$ (mm^2/s)
Couette flow	46.1	4.90	11.5	–11.5	46.1
Poiseuille flow	44.7	4.74	7.4	–14.8	44.7
Second-order shear flow	70.3	7.48	17.5	–17.5	70.3
Sine flow	37.7	4.00	9.35	–9.35	37.7
Cosine flow	37.7	4.00	9.35	–9.35	37.7
Stagnant	0.288	–	0	0	0.288

same rate once the fronts have converged. Thus we can answer one of our initial questions: even when K is held constant, varying the velocity profile $u(y)$ does affect the product generation rate.

With these converged growth rates in mind, we define a dimensionless efficiency of reactive mixing:

$$\eta = \frac{\frac{\partial A}{\partial t} - v_0 p_0}{(hK)^{1/2}}, \tag{6}$$

where p_0 is the initial perimeter of the reacted region (total length of the fronts). In stagnant fluid, the reacted region grows at rate $v_0 p_0$, so η measures the increase in the growth rate beyond that of stagnant fluid, normalized by the domain size h and total kinetic energy K. A flow that generates a reaction product no faster than stagnant fluid would have $\eta = 0$; a flow that generates a reaction product slower than stagnant fluid would have $\eta < 0$; a flow that generates product much faster, while requiring little kinetic energy, would have $\eta \gg 1$. In stagnant flow, η is undefined, since $\partial A/\partial t = v_0 p_0$ and $K = 0$. In all cases considered here, $p_0 = 2h$, but Eq. (6) could be generalized to more complicated geometries. Table II lists the reactive mixing efficiency of each of the six cases. By definition, they rank in the same order as for $\partial A/\partial t$.

III. ANALYTIC MODEL

The simulation results of Sec. II show that fronts converge over time to stable shapes, and once they have converged, reacted regions grow at constant rates. But what determines the curious solitary wave shapes shown in Fig. 4? Insight can be gained by considering the speed at which solitary waves advance. In each of the six cases simulated, the converged growth rate of the reacted region depends on the maxima and minima of the corresponding velocity profile, $u_{\max}$ and $u_{\min}$. As the table shows, in every case,

$$\frac{\partial A}{\partial t} = h(2v_0 + u_{\max} - u_{\min}).$$

In words, each reacted region grows at a rate consistent with its rightward front advancing at the maximum possible speed $u_{\max} + v_0$ and its leftward front advancing at the maximum possible speed $|u_{\min}| + v_0$. That idea is consistent with prior predictions [23] and observations [25] considering Poiseuille flow. Fronts advance at maximum possible speeds when they are pinned to leading elements. If ever a front element with angle $\theta = \pi/2$ reaches a location $y_{\max}$ of maximum (rightward) flow velocity $u_{\max}$, then that element will advance rightward at maximum speed, leading all others. The mechanism is similar to a front in an opposing flow pinning to a slow zone and thus freezing in place, as observed previously [13,27,28]. The reacted region will spread laterally from the leading element, so that once converged, the whole front will move at the same speed as the leading element. Thus, over an interval dt, the location where a converged front intersects an arbitrary line $y = y_0$ will advance by a distance

$$dx = dt(u_{\max} + v_0). \tag{7}$$

However, the velocity of an individual *front element* need not be strictly in the $\hat{\boldsymbol{x}}$ direction, because advection can displace elements along the curve of the front without changing its apparent shape or position. (Elements moving this way have previously been called "sliding fronts" [13].) Over an interval dt, a front element in stagnant fluid and oriented at angle θ advances a distance $v_0\,dt$ in the direction $\theta - \pi/2$, as shown in Fig. 6. Assuming adjacent elements are also oriented at angle θ, over the same interval, the location where the front intersects $y = y_0$ advances by a distance $dt\,v_0/\cos(\theta - \pi/2) = dt\,v_0/\sin\theta$. If the fluid is not stagnant but has velocity $\boldsymbol{u} = u\hat{\boldsymbol{x}}$, then superposition holds according to Eq. (3), and over the same interval, the location where the front intersects $y = y_0$ advances by a distance

$$dx = dt\left(u + \frac{v_0}{\sin\theta}\right). \tag{8}$$

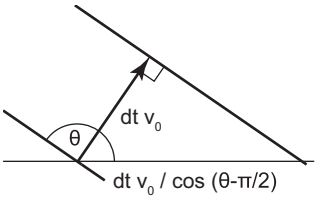

FIG. 6. Geometry of an advancing front in stagnant fluid ($\boldsymbol{u} = 0$). Over an interval dt, each front element advances a distance $dt\,v_0$ in the direction $\theta - \pi/2$, so that the location where the front intersects $y = y_0$ advances a distance $dt\,v_0/\cos(\theta - \pi/2)$.

Comparing Eqs. (7) and (8), we see that for a solitary wave,

$$\sin\theta = \frac{v_0}{u_{\max} - u + v_0}.$$

From this expression we can use similar triangles to show

$$\frac{\partial x}{\partial y} = \pm\left[\left(\frac{u_{\max} - u}{v_0} + 1\right)^2 - 1\right]^{1/2}, \tag{9}$$

with the sign taken to match the sign of $(y - y_{\max})/(u - u_{\max})$.

By analogous reasoning, if ever a front element with angle $\theta = -\pi/2$ reaches a location $y_{\min}$ of minimum flow velocity $u_{\min}$ (maximum leftward flow speed), then that element will advance leftward at maximum speed, leading all other elements and forming a leftward solitary wave governed by an expression analogous to Eq. (9),

$$\frac{\partial x}{\partial y} = \pm\left[\left(\frac{u_{\min} - u}{v_0} - 1\right)^2 - 1\right]^{1/2}, \tag{10}$$

with the sign taken to match the sign of $(y - y_{\min})/(u - u_{\min})$.

Both expressions are consistent with our expectations for limiting cases. If $v_0 \ll U$, then $\partial x/\partial y \to \infty$, so the front lies along the flow. In this case, the flow speed dominates the chemical speed, and fronts can converge only if they are severely (infinitely) stretched in the flow direction. Alternately, if $v_0 \gg U$, then $\partial x/\partial y = 0$, so the front lies across the flow. In this case, the chemical speed dominates the flow speed, so that the flow effects are negligible, and the front propagates as if it were in stagnant fluid. Numerical solutions of Eqs. (5) with varying values of the chemical front velocity v_0 show solitary wave shapes consistent with these expectations, as shown in Fig. 7.

By integrating either Eq. (9) or Eq. (10), we can predict the shape of any solitary wave. The results of such calculations, for both leftward and rightward fronts subjected to the flows listed in Table I, are shown in Fig. 8. The shapes calculated using Eqs. (9) and (10) closely match the results of simulating Eq. (3), even at cusps. That agreement provides strong support for the idea that solitary waves are pinned to leading elements.

In all the flows listed in Table I, and in any flow that can be written in the form $\boldsymbol{u} = u(y)\hat{\boldsymbol{x}}$, the phenomenon of fronts pinning to leading elements implies that at long times, the bulk reaction rate is governed by only the chemical kinetics (encoded in v_0) and the extrema of the velocity profile ($u_{\max}$ and $u_{\min}$). Other features of the velocity profile are irrelevant. After fronts have converged, kinetic energy in the flow anywhere other than the leading element has no effect and therefore decreases the efficiency of reactive mixing. Here we can answer another of our initial questions: sharper velocity profiles drive more efficient autocatalytic mixing. Accordingly, the most efficient of the six flows considered here is the second-order shear flow (see Table II)

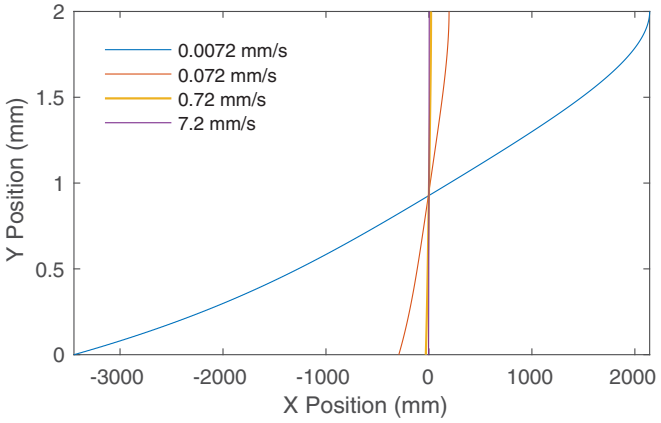

FIG. 7. Influence of chemical speed on shape of the rightward solitary wave in second-order shear flow. Larger chemical speeds reduce the relative importance of flow, flattening the front, whereas smaller chemical speeds increase the relative importance of flow and particularly shear, extending the front streamwise. The trend is consistent with Eqs. (9) and (10).

because the extrema of its velocity profile exceed those of the other five flows (Fig. 1 and Table II).

With these dynamics in mind, we can construct a flow whose reactive mixing efficiency is greater than any other considered here—and almost any possible flow—if we concentrate the kinetic energy at one element of the leftward front and one element of the rightward front. The resulting velocity profile would have zero mean flow, consistent with the other cases. Such a profile might be constructed using the Dirac δ function $\delta(y)$, but the speeds and shear rates would be infinite and therefore nonphysical, and calculating the kinetic energy would be mathematically problematic since $\delta^2(y)$ is ill-defined. A near-optimal flow that can in principle be realized in physical systems

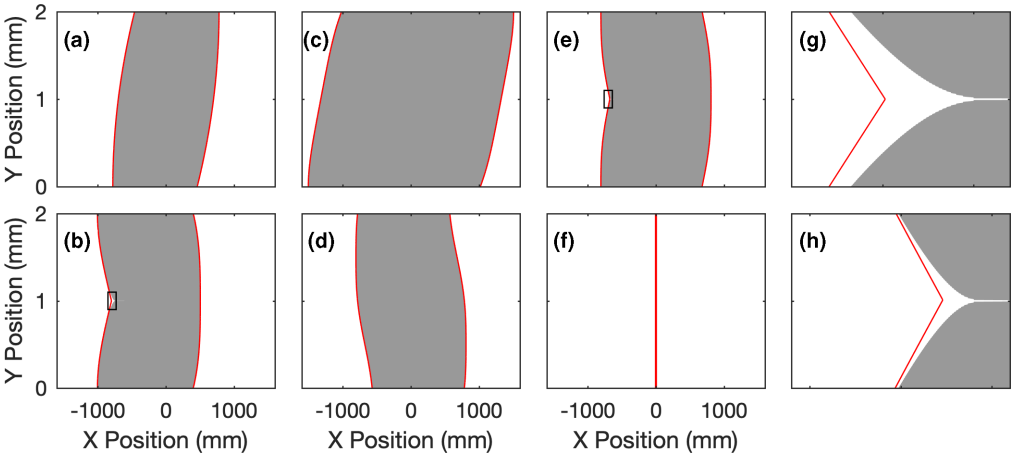

FIG. 8. Solitary wave shapes in the six flows considered, with eikonal simulation results at $t = 67.6$ s (repeated from Fig. 4) shown as gray regions and analytic predictions shown as red curves: (a) Couette flow, (b) Poiseuille flow, (c) second-order shear flow, (d) sine flow, (e) cosine flow, (f) stagnant fluid, (g) enlargement of cusp region in Poiseuille flow, and (h) enlargement of cusp region in cosine flow. Analytic predictions match eikonal results closely, especially when far from cusps.

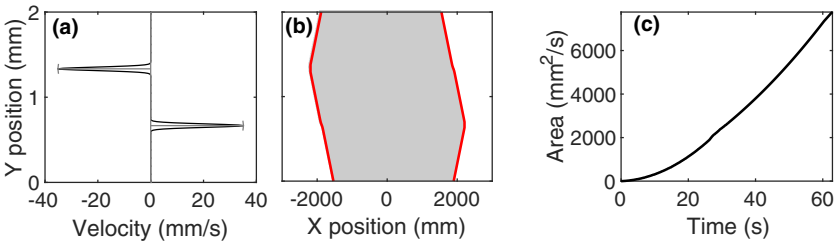

FIG. 9. Reactive mixing by the double-Gaussian flow specified in Eq. (11), with $(\sigma, y_R, y_L) = (h/100, h/3, 2h/3)$: (a) velocity profile, (b) reacted region after fronts have converged, along with the front shapes predicted by Eqs. (9) and (10), shown in red. Note that the reacted region is wider than any shown in Fig. 8. (c) Growth of the reacted region over time. The double-Gaussian flow converges to a faster growth rate than any of the flows shown in Fig. 1. Its efficiency for reactive mixing is nearly optimal.

and is mathematically tractable is the double-Gaussian flow given by

$$u(y) = \left(\frac{K}{\sigma}\right)^{1/2} \pi^{-1/4} \left(e^{-\frac{(y-y_R)^2}{2\sigma^2}} - e^{-\frac{(y-y_L)^2}{2\sigma^2}}\right), \tag{11}$$

which concentrates kinetic energy in two narrow regions of width $\sigma \ll h$, one centered at $y = y_R$ and moving rightward, the other centered at $y = y_L$ and moving leftward. In the limit $\sigma \to 0$, it approximates two δ functions. The extrema of the velocity profile are $u_{\max} = (K/\sigma)^{1/2}\pi^{-1/4}$ and $u_{\min} = -(K/\sigma)^{1/2}\pi^{-1/4}$, so after the fronts converge, the growth rate of the reacted region is $\partial A/\partial t = 2hv_0 + 2h(K/\sigma)^{1/2}\pi^{-1/4}$ and the efficiency is

$$\eta = \frac{2}{\pi^{1/4}}\sqrt{\frac{h}{\sigma}}.$$

As expected, the efficiency is high when $\sigma \ll h$, meaning that energy is highly concentrated in the two narrow regions.

Figure 9 shows the velocity profile of this near-optimal flow, with $(\sigma, y_R, y_L) = (h/100, h/3, 2h/3)$, as well as the results of simulating fronts in the flow and the results of calculating the converged front shape using Eqs. (9) and (10). The two approaches agree closely. For these parameters, $u_{\max} = 31.5$ mm/s and $u_{\min} = -31.5$ mm/s. Theory predicts the reacted region to grow at a rate of 140.7 mm^2/s, and at long times, we measure its growth rate to be 141.0 mm^2/s. Accordingly, the predicted efficiency after convergence is 15.035, and the measured value is 15.067. Analytic predictions again match simulation results closely. The growth rate and reactive mixing efficiency of this double-Gaussian flow are more than double the values of any cases listed in Table II, and would be greater still if we chose σ smaller.

In any reactive flow governed by these dynamics, the shape of the velocity profile is irrelevant for predicting the bulk reaction rate at long times; only its extrema matter. But the shape does affect reaction rates at short times. Before the global leading element, which advances faster than any other, comes to dominate the entire front, local leading elements can dominate their local neighborhoods. A reacted region spreads laterally from each, and the spreading cannot depend on advection, which has no lateral component, so we would expect the spreading speed to be v_0 and the global convergence time to be on the order of h/v_0. Table III lists the convergence times for fronts in the flows shown in Fig. 1. For each, the convergence time is defined as the time after which $\partial A/\partial t$ stays within 1% of its long-term value. All are of the same order of magnitude as $h/v_0 = 28$ s for the parameters considered here. Cosine flow and Poiseuille flow converge fastest, consistent with the fact that their leading elements lie on the centerline and the entire domain lies within distance $h/2$. In stagnant fluid, every element on any front is a leading element, so convergence is immediate. Other convergence times are substantially longer than h/v_0, however. High-accuracy prediction of

TABLE III. Front convergence times.

Description	Convergence time (s)
Couette flow	25.1
Poiseuille flow	14.00
Second-order shear flow	39.3
Sine flow	53.8
Cosine flow	11.63
Double-Gaussian flow	62.4
Stagnant	0

convergence time may be frustrated by the presence of cusps and therefore require simulating the full advection-reaction-diffusion dynamics, as discussed below.

Fronts that converge over time and then advance at constant speed are consistent with solitary waves pinning to leading elements advancing at speed $u_{\max} + v_0$ or $|u_{\min}| + v_0$. A related phenomenon, seen in prior studies with simulations and experiments [16,29] considering opposing flows, is the pinning of fronts to elements that hold their position over time. In flows of the form $\boldsymbol{u} = u(y)\hat{\boldsymbol{x}}$, frozen fronts are constrained by $u + v_0/\sin\theta = 0$ [compare to Eq. (8)], so by reasoning analogous to what produced Eq. (9), their shapes can be calculated by integrating

$$\frac{\partial x}{\partial y} = \pm\left(\frac{u^2}{v_0^2} - 1\right)^{1/2}. \tag{12}$$

This expression matches Eq. (6) of Chevalier *et al.* [16] if the spanwise flow component is zero ($v_y = 0$, in their notation) and curvature effects are neglected ($l_\chi = 0$, in their notation). This expression also matches that used to produce the fit curve in Fig. 5 of Atis *et al.* [28] (though the vertical axis of that figure should be labeled, in their notation, $\theta/2$, not θ). Frozen fronts are a specific case of solitary waves. We expect that the shapes of frozen fronts observed in other experiments [27] and simulations [13] could likewise be reproduced by integrating an expression like Eq. (12) that included spanwise flow.

Another related phenomenon occurs when a front propagates in a flow that opposes it everywhere and is fast enough to drive it backward [28]. We hypothesize that such a front eventually converges to a solitary wave moving with constant speed. For a rightward ($\theta = \pi/2$) front being driven in the $-\hat{\boldsymbol{x}}$ direction, that speed will be $u_{\max} + v_0$, where $u_{\max} < -v_0 < 0$, and its shape will be set by Eq. (9). For a leftward ($\theta = -\pi/2$) front being driven in the $+\hat{\boldsymbol{x}}$ direction, that speed will be $u_{\min} - v_0$, where $0 < v_0 < u_{\min}$, and its shape will be set by Eq. (10). Future work might test these hypotheses.

IV. ADVECTION-REACTION-DIFFUSION SIMULATION

The results described in Sec. II come from simulating reactive mixing according to the simplified dynamics given by Eqs. (5), not the full dynamics given by Eq. (2). Likewise, the analytic predictions described in Sec. III come from geometric reasoning built on the same simplification. Though we expect the simplified dynamics to closely approximate the full dynamics when $\mathrm{Da_{II}} \gg 1$, which is true for all the cases considered here, the simplification should nonetheless be validated.

To validate the results and theory described so far, we numerically solved Eq. (2) for the second-order shear and Poiseuille flows described in Table I using a first-order central-differences algorithm on a regular, rectangular grid with Eulerian time stepping. We chose $D = 1.0 \times 10^{-3}$ mm^2/s, and $\alpha = 1.2$ s^{-1} ($\mathrm{Da_{II}} = 4800$), consistent with the value of the chemical velocity v_0 used for eikonal simulations (see Sec. II). The domain spanned $0 \leqslant y \leqslant h$ (keeping $h = 2$ mm as above) and $-x_{\max} \leqslant x \leqslant x_{\max}$, with $x_{\max}$ adjusted for each simulation to ensure that the reacted region did

not reach the left or right boundaries. Grid points were spaced $dx = 0.05$ mm in the x direction and $dy = 0.005$ mm$= 0.0025h$ in the y direction. The time step dt was chosen according to the Courant-Friedrichs-Lewy condition $dt = 0.15\,dy/u_{\max}$, which tests revealed to be small enough for good stability. We imposed the Neumann boundary condition $\partial c/\partial y = 0$ at $y = 0$ and $y = h$. The initial product concentration was

$$c_0 = \begin{cases} \frac{1}{(1+e^{-(x+\mu)/L})^2}, & x \leqslant 0 \\ \frac{1}{(1+e^{(x-\mu)/L})^2}, & x > 0 \end{cases}, \tag{13}$$

where $\mu = 20$ mm$= 10h$ and $L = \sqrt{6D/\alpha}$, so that the initial concentration profile is the superposition of two solitary waves in the absence of advection, separated by distance 4μ. We continued the simulation long enough for the shape and growth rate of the reacted region to converge.

The resulting concentration for second-order shear flow is animated in the Supplemental Material, movie S2 [22], and shown in Fig. 10. As expected, the reacted region initially grows fastest near $y = 0$ and $y = h$, where the second-order shear flow is fastest. Over time, lateral spreading from each of the two leading points broadens those parts of the reacted region, until finally a converged shape emerges and persists thereafter. That spreading and convergence is consistent with the solitary waves we observed in eikonal simulations, shown in Figs. 2 and 4. Where those parts intersect, the eikonal approximation predicts overlapping fronts forming a corner with discontinuous slope, as visible in Fig. 2. Under advection-reaction-diffusion dynamics, concentration varies continuously and smoothly, but where those parts intersect, concentration varies over much smaller length scales than elsewhere. We observe defects marking the edge of the region of influence of each leading element, as shown in the inset of Fig. 10. They spread laterally across the domain over time, as expected. Defects indicate that the fine-scale structures of the local concentration are not well resolved; a higher simulation resolution would resolve them but is unnecessary for demonstrating lateral spreading, which is already evident.

In Sec. II, we considered the growth of the reacted area. For comparison, we define the reacted region in advection-reaction-diffusion simulations as the region between the leftmost and rightmost points where $c \geqslant 0.5$. Its area grows over time and is plotted in Fig. 11. The figure also shows variation of the area of the reacted region in an eikonal simulation of the same flow, with corresponding initial conditions. (That is, at $t = 0$, the rightward front had $\theta = \pi/2$ and laid on the line $x = 40$ mm, while the leftward front had $\theta = -\pi/2$ and laid on the line $x = -40$ mm. In contrast, all fronts considered in Sec. II started on the line $x = 0$, but an initially reacted region of zero size is nonphysical for advection-reaction-diffusion simulations.) The eikonal simulation produces a reacted region that is bigger by about 10%. Our primary interest is the long-term rate of product generation, and at large times, both regions grow at similar rates. In second-order shear flow, the converged growth rates are 70.3 mm^2/s for the eikonal simulation (as in Table II) and 70.1 mm^2/s for the advection-reaction-diffusion simulation. Similarly, there was close correlation for Poiseuille flow at large times: 44.7 mm^2/s for the eikonal simulation and 44.1 mm^2/s for the advection-reaction-diffusion simulation. Thus eikonal simulations, with computational cost much less than advection-reaction-diffusion simulations, are moderately accurate for predicting the instantaneous size of the reacted region, and quite accurate for predicting converged growth rates.

Up to now, the area of the reacted region has served as a surrogate for a quantity of more practical interest, the total mass of product. However, simulating the full advection-reaction-diffusion dynamics gives us direct access to the product mass,

$$m = \int \rho c \, dV, \tag{14}$$

where in these two-dimensional systems the integration is over the entire area, and we assume the density ρ is a known constant. Figure 11 shows the variation of product mass (normalized by ρ) over time, which closely follows the reacted area estimated from eikonal and advection-reaction-diffusion simulations, consistent with the fact that fronts are narrow in the $\mathrm{Da_{II}} \gg 1$ limit.

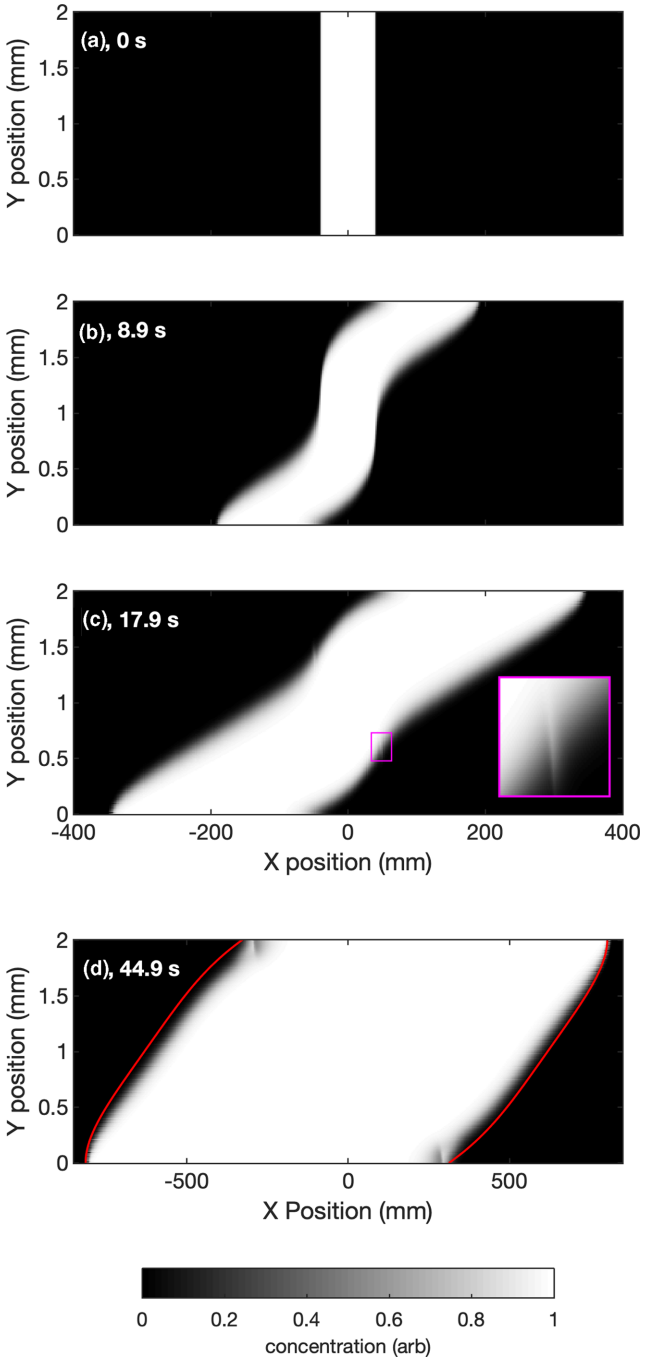

FIG. 10. Concentration of reaction product evolving over time according to advection-reaction-diffusion dynamics in second-order shear flow. The simulation begins with a stripe-shaped region where $c = 1$ (a), which widens and changes shape (b–c), converging on a steady shape at long times (d). The analytic predictions of solitary chemical wave shape [from Eqs. (9) and (10), repeated from Fig. 4, and plotted in red] approximate the converged shape reasonably well. The inset in (c) shows an enlargement of the boxed region, containing a defect corresponding to one of the cusps in Fig. 2. The same evolution of concentration is animated in Supplemental Material, movie S2 [22].

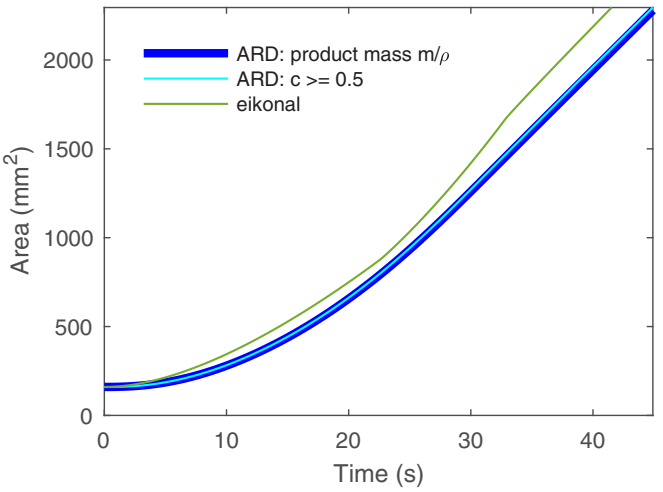

FIG. 11. Growth of the reacted region in second-order shear flow, from eikonal (repeated from Fig. 5) and advection-reaction-diffusion simulations. The eikonal simulation predicts a reacted region slightly larger than the actual region that results from the advection-reaction-diffusion simulation. In the advection-reaction-diffusion simulation, the normalized mass m/ρ from Eq. (14) closely matches the area marked by $c \geqslant 0.5$. At long times, all three quantities grow at similar rates.

In second-order shear flow, at long times, the growth rate of the normalized mass is 70.3 mm^2/s, closely matching the growth rates of the reacted regions in both eikonal and advection-reaction-diffusion simulations.

The converged efficiency of reactive mixing η [Eq. (6)] in the advection-reaction-diffusion equation can be calculated using either the area defined from $c \geqslant 0.5$ or the normalized mass; in second-order shear flow the resulting values are 7.47 and 7.48, respectively. Both closely agree with $\eta = 7.48$ from eikonal simulation (Table II). The corresponding convergence times are 28.4 and 29.4 s, respectively. Thus the advection-reaction-diffusion simulation predicts significantly faster convergence than the eikonal simulation, where the convergence time was 39.3 s ($\tilde{t} = 130$), as shown in Table III. That disagreement is consistent with the growth dynamics shown in Fig. 11. Both curves produced by the advection-reaction-diffusion equation converge smoothly, but the curve produced by the eikonal simulation overshoots before an inflection point at 33 s ($\tilde{t} = 109$), after which it rapidly converges. As shown in the Supplemental Material, movie S1 [22], cusps are eliminated from the fronts at 33 s, so we attribute the slow convergence to their presence. We expect the convergence times predicted by advection-reaction-diffusion simulations to be significantly more accurate than those predicted by eikonal simulations.

Finally, we can compare the front shapes predicted by the analytic model presented in Sec. III to the results of the advection-reaction-diffusion simulation. The last panel of Fig. 10 shows a concentration field from late in the second-order shear flow simulation, after solitary wave shapes have converged, along with the shapes predicted by Eqs. (9) and (10). The analytic model predicts fronts encompassing an area a few percent larger than the region where $c \geqslant 0.5$ in the advection-reaction-diffusion results, consistent with the results shown in Fig. 11. A similar mismatch was previously observed in simulations of solitary waves with speed zero and was attributed to a dependence of front speed on front thickness [16]. The same mechanism may be responsible here, and the variation of front speed with front thickness is a fruitful topic for further study. Nonetheless, considering the simplicity of our geometric arguments and the fact that calculating shapes according to our prediction requires many orders of magnitude less computing time than performing the advection-reaction-diffusion simulation, the analytic prediction may prove useful.

V. CONCLUSION

In this paper, we have explored a question motivated by the design of industrial mixers: For a given kinetic energy, what laminar, two-dimensional flow drives autocatalytic reactive mixing most efficiently, that is, generates reaction product at the greatest rate? Using the eikonal approximation, we started by simulating the dynamics of chemical reaction fronts in stagnant fluid and in five laminar flows: Couette flow, Poiseuille flow, second-order shear flow, sine flow, and cosine flow. We found that fronts converged at long times to fixed shapes that propagated at constant speed—solitary waves. That observation had been made previously for Poiseuille flow, and we found it to be true in every flow considered. We found those shapes to be dynamically stable in that small perturbations decay away over time. Because the propagation speeds were different for different flows, they generated a reaction product at different rates. Noting that those converged rates depend only on the inherent chemical front speed and the extrema of the velocity profile, we used geometric arguments to produce an analytic prediction for the solitary wave shapes. The predicted shapes closely match simulation results. Moreover, because the converged rates depend on no characteristic of the velocity profile except its extrema, we hypothesized that a flow with its kinetic energy concentrated in narrow regions would generate reaction product fastest. We confirmed that hypothesis by simulating such a flow, and our analytic model accurately predicted the shape of the resulting solitary wave. Our analytic model, in the particular case of solitary waves moving at speed zero, matches prior studies of frozen fronts. Finally, for validation we simulated the second-order shear flow using the full advection-reaction-diffusion dynamics (not the simplified dynamics of fronts that results from the eikonal approximation). Generally, we found good agreement between the two simulations; instantaneous areas match within about 10%, and converged product generation rates matched within about 0.1%.

The applicability of our findings is limited primarily by our choice to study flows that are strictly streamwise, and therefore lacking vortices, spatial oscillation, and vorticity. We expect that eikonal simulations could accurately predict the product generation rates of flows with greater geometric complexity, and one recent study used the same code to show that eikonal simulations closely match experiments in a similar context [17]. Still, we have not validated our expectation in the context of product generation rates. Interestingly, Mahoney *et al.* [13] reported that multiple frozen front shapes were possible in the same flow, depending on the initial conditions. We speculate that this degeneracy of frozen front shapes is enabled by the presence of vorticity (or at least spanwise flow) and that the same would be true for solitary waves with nonzero speed. Generalizing Eqs. (9), (10), and (12) to include spanwise flow might allow a test. That said, the notion of convergence is not so easy to define for flows that vary along the direction of growth of the reacted region. We also speculate that burning invariant manifolds [24,30] and burning Lagrangian coherent structures [31] could be explained as the locations that admit the existence of solitary waves of speed zero.

The applicability of our findings is further limited by our choice to study two-dimensional flows. Three-dimensional flows involve more degrees of freedom and a wider variety of mechanisms for chaotic mixing [32]. Three-dimensional flows also differ from two-dimensional flows profoundly in other aspects of their physics, such as the direction of the turbulent energy cascade [33]. Thus product generation rates might be qualitatively different. Making an analytic model to predict solitary wave shapes in arbitrary three-dimensional flows would be significantly more difficult because so many more topological features are possible in three dimensions than in two [34]. However, we expect that our existing analytic model could be readily generalized to strictly streamwise flows in three-dimensional domains. Future work could test this conjecture.

Flows that vary in time would also complicate the dynamics, as shown in a prior study of pulsing Poiseuille flow [26]. Adding time dependence might also introduce new interactions with the three existing timescales (advection, reaction, and diffusion), such as resonances. Streamwise, laminar, steady flows do closely approximate flows observed in some contexts, especially when the Reynolds number is low.

Our approach is limited to reactions whose kinetics allow stationary waves in stagnant fluid, thereby justifying the eikonal approximation. We have focused on autocatalytic second-order reactions specifically, though stationary waves can also occur for first-order reactions [$F(c) = c$], and our approach applies to any chemical system where the eikonal approximation is accurate. Allowing feedback from the reaction dynamics of Eq. (2) to the underlying flow $\boldsymbol{u}$ might make our line of reasoning applicable to systems where flow is affected by the generation of heat or reaction products of differing density.

The eikonal approximation, as we have stated it, is accurate only if both Damköhler numbers are large and front curvature is not too great. Those caveats put important limits on the double-Gaussian flow that we found to be nearly optimal for autocatalytic reactive mixing, according to simulations and analytic reasoning based on the eikonal approximation. We found that the reactive mixing efficiency increases steadily as kinetic energy is concentrated into a smaller and smaller region. But the sharpness of that region would induce extreme front curvature at its tip; the narrower the region, the less accurate the eikonal approximation will be. Including a curvature term in Eq. (3) might improve accuracy. Furthermore, we have restricted our study to second-order autocatalytic chemical kinetics of the form $F(c) = c(1 - c)$, but many other sorts of chemical kinetics are possible. In particular, under third-order autocatalytic kinetics of the form $F(c) = c(1 - c)(c - c_0)$, where c_0 is a constant, if the combined effects of advection and diffusion drive the local concentration below c_0, the chemical kinetics will tend to reduce concentration to zero. Such reactions generate product most quickly when the local strain lies within an optimal range [35,36]. For them, concentrating kinetic energy into the smallest possible region would not optimize product generation; rather, it would blow out the reaction. We expect that higher shear would also alter the front thickness, which would affect the front speed, as mentioned above.

We hope that the results presented in this paper provide useful strategies for producing efficient autocatalytic mixing, as well as insights into the underlying mechanisms.

ACKNOWLEDGMENTS

The authors are grateful for fruitful conversations with K. A. Mitchell and I. A. Mohammad. T.D.N. was supported by the Department of Defense through the National Defense Science & Engineering Graduate Fellowship (NDSEG) Program.

[1] S. M. Kresta, V. A. Atiemo-Obeng, E. L. Paul, and V. Atiemo-Obeng, *Handbook of Industrial Mixing: Science and Practice* (John Wiley & Sons, Hoboken, NJ, 2004).

[2] N. Harnby, M. F. Edwards, and A. W. Nienow, *Mixing in the Process Industries*, 2nd ed. (Butterworth-Heinemann, Oxford, 1997).

[3] G. Ascanio, Mixing time in stirred vessels: A review of experimental techniques, Chin. J. Chem. Eng. **23**, 1065 (2015).

[4] W. G. Yao, H. Sato, K. Takahashi, and K. Koyama, Mixing performance experiments in impeller stirred tanks subjected to unsteady rotational speeds, Chem. Eng. Sci. **53**, 3031 (1998).

[5] N. Di Patrizio, M. Bagnaro, A. Gaunand, J.-F. Hochepied, D. Horbez, and P. Pitiot, Hydrodynamics and mixing performance of Hartridge Roughton mixers: Influence of the mixing chamber design, Chem. Eng. J. **283**, 375 (2016).

[6] E. Lunasin, Z. Lin, A. Novikov, A. Mazzucato, and C. R. Doering, Optimal mixing and optimal stirring for fixed energy, fixed power, or fixed palenstrophy flows, J. Math. Phys. **53**, 115611 (2012).

[7] C. Seis, Maximal mixing by incompressible fluid flows, Nonlinearity **26**, 3279 (2013).

[8] D. P. G. Foures, C. P. Caulfield, and P. J. Schmid, Optimal mixing in two-dimensional plane Poiseuille flow at finite Péclet number, J. Fluid Mech. **748**, 241 (2014).

[9] M. Farazmand, Optimal initial condition of passive tracers for their maximal mixing in finite time, Phys. Rev. Fluids **2**, 054601 (2017).

[10] Z. Neufeld and E. Hernndez-Garca, *Chemical and Biological Processes in Fluid Flows: A Dynamical Systems Approach* (World Scientific, Singapore, 2009).
[11] R. A. Fisher, The wave of advance of advantageous genes, Annals of Eugenics **7**, 355 (1937).
[12] A. N. Kolmogorov, I. G. Petrovskii, and N. S. Piskunov, Étude de l'equation de la diffusion avec croissance de la quantité de matière et son aplication à un probléme biologique, Bulletin de l'Uversité d'Etat à Moscou, Ser. Int., Sect. A **1**, 1 (1937).
[13] J. R. Mahoney, J. Li, C. Boyer, T. Solomon, and K. A. Mitchell, Frozen reaction fronts in steady flows: A burning-invariant-manifold perspective, Phys. Rev. E **92**, 063005 (2015).
[14] R. S. Spangler and B. F. Edwards, Poiseuille advection of chemical reaction fronts: Eikonal approximation, J. Chem. Phys. **118**, 5911 (2003).
[15] S. Gowen and T. Solomon, Experimental studies of coherent structures in an advection-reaction-diffusion system, Chaos **25**, 087403 (2015).
[16] T. Chevalier, D. Salin, and L. Talon, Frozen fronts selection in flow against self-sustained chemical waves, Phys. Rev. Fluids **2**, 043302 (2017).
[17] T. D. Nevins and D. H. Kelley, Vertical shear alters chemical front speed in thin-layer flows, J. Fluid Mech. **874**, 235 (2019).
[18] P. M. Wood and J. Ross, A quantitative study of chemical waves in the Belousov Zhabotinsky reaction, J. Chem. Phys. **82**, 1924 (1985).
[19] R. J. Field and R. M. Noyes, Oscillations in chemical systems, IV. Limit cycle behavior in a model of a real chemical reaction, J. Chem. Phys. **60**, 1877 (1974).
[20] R. M. Noyes and R. J. Field, Oscillatory chemical reactions, Annu. Rev. Phys. Chem. **25**, 95 (1974).
[21] T. D. Nevins and D. H. Kelley, Front tracking for quantifying advection-reaction-diffusion, Chaos **27**, 043105 (2017).
[22] See Supplemental Material at http://link.aps.org/supplemental/10.1103/PhysRevFluids.5.063201 for movies showing the evolution of fronts in an eikonal simulation and the evolution of concentration in an advection-diffusion simulation.
[23] B. F. Edwards, Poiseuille Advection of Chemical Reaction Fronts, Phys. Rev. Lett. **89**, 104501 (2002).
[24] K. A. Mitchell and J. R. Mahoney, Invariant manifolds and the geometry of front propagation in fluid flows, Chaos **22**, 037104 (2012).
[25] M. Leconte, J. Martin, N. Rakotomalala, and D. Salin, Pattern of Reaction Diffusion Fronts in Laminar Flows, Phys. Rev. Lett. **90**, 128302 (2003).
[26] M. Leconte, N. Jarrige, J. Martin, N. Rakotomalala, D. Salin, and L. Talon, Taylor's regime of an autocatalytic reaction front in a pulsative periodic flow, Phys. Fluids **20**, 057102 (2008).
[27] M. E. Schwartz and T. H. Solomon, Chemical Reaction Fronts in Ordered and Disordered Cellular Flows with Opposing Winds, Phys. Rev. Lett. **100**, 028302 (2008).
[28] S. Atis, S. Saha, H. Auradou, D. Salin, and L. Talon, Autocatalytic Reaction Fronts Inside a Porous Medium of Glass Spheres, Phys. Rev. Lett. **110**, 148301 (2013).
[29] S. Saha, S. Atis, D. Salin, and L. Talon, Phase diagram of sustained wave fronts opposing the flow in disordered porous media, EPL **101**, 38003 (2013).
[30] J. Mahoney, D. Bargteil, M. Kingsbury, K. Mitchell, and T. Solomon, Invariant barriers to reactive front propagation in fluid flows, EPL **98**, 44005 (2012).
[31] J. R. Mahoney and K. A. Mitchell, Finite-time barriers to front propagation in two-dimensional fluid flows, Chaos **25**, 087404 (2015).
[32] J. M. Ottino, Mixing, chaotic advection, and turbulence, Annu. Rev. Fluid Mech. **22**, 207 (1990).
[33] G. Boffetta and R. Ecke, Two-dimensional turbulence, Annu. Rev. Fluid Mech. **44**, 427 (2012).
[34] A. E. Perry and M. S. Chong, A description of eddying motions and flow patterns using critical-point concepts, Annu. Rev. Fluid Mech. **19**, 125 (1987).
[35] T. D. Nevins and D. H. Kelley, Optimal Stretching in Advection-Reaction-Diffusion Systems, Phys. Rev. Lett. **117**, 164502 (2016).
[36] J. Wang, J. Tithof, T. D. Nevins, R. O. Colón, and D. H. Kelley, Optimal stretching in the reacting wake of a bluff body, Chaos **27**, 123109 (2017).